UNIVERSITY OF GRONINGEN

BACHELOR RESEARCH PROJECT

Simulating ToF spectra of H_2 ion fragments, as produced by Sn^{5+} – H_2 interactions

Author:
Lukas Raap *(S3434494)*

Daily supervisor:
Subam Rai, MSc
First supervisor:
prof. dr. ir. R. Hoekstra
Second supervisor:
dr. T. Schlathölter

Friday 26th February, 2021

1 Abstract

In this research project, we investigate the Time of Flight (ToF) spectrum of ionic H_2 fragments who are created in collisions between high-energy Sn ions and H_2 molecules. CHEOPS, the experimental setup used to investigate such interactions is equipped with a ToF spectrometer to perform mass spectrometry on the ionic H_2 fragments. Besides determining the detection efficiency for the ionic fragments, we aim to measure kinetic energies involved in the collision. To achieve this goal, a model of the experimental setup is constructed using SIMION. Particle trajectories are then simulated, and benchmarked to experimental data.
Flight times of the ions are excellently reproduced. The transmission and detection efficiencies which differ significantly from simple analytical approximations are in fair agreement and in much better agreement than the analytical results.

Contents

2 Introduction

Until the end of world war II, most electronic devices used vacuum tubes as switches. These large, energy-consuming components were slowly phased out in favour of solid state transistors [1]. In 1947 the first functioning transistor was made at Bell Laboratories, for which the creators were awarded the 1956 Nobel Prize. Three years later, in 1959, another advancement in solid state physics was made when the Metal-Oxide-Semiconductor Field-Effect Transistor (MOSFET) was invented, also at Bell Laboratories [1].
These new devices proved to be sufficiently superior to the old vacuum tubes to not only replace them, but to surpass them by a large margin and bring about the information era we are currently living in.

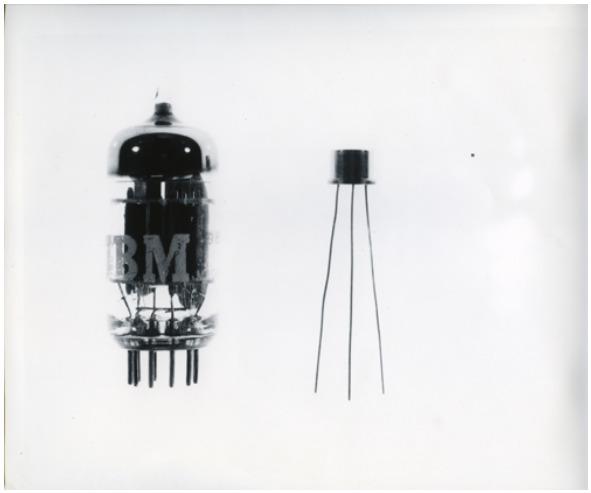

Figure 1: An early transistor (circa 1964) compared to a vacuum tube. Note the difference in size. Image adapted from [2]

Two of the biggest advantages over vacuum tubes for MOSFETs is the fact that they require a lot less power [1], and the ease with which they can be miniaturized, see figure 1 for a comparison between a vacuum tube and an early transistor. Another is that they can be made into integrated circuits, where many transistors are made out of the same wafer. This saves space and assembly time, which made transistors cheap and affordable to the general public.
All of these qualities lead to the miniaturization of transistors, whose ever decreasing size has been described in Moore's law, all the way back in 1965. Simply put, it states that the number of transistors on a silicon chip doubles roughly every 2 years [3].
In order to stick to the prediction, transistors need to become increasingly smaller, which means the etching size on wafers needs to slim down as well. In order to understand how that is done, we need to first understand the basics of current silicon chip manufacturing [4], which is done using a process called photo-lithography, which is illustrated in figure 2.
First, the top of a mono-crystalline silicon wafer substrate is oxidized at high temperatures to passivize the wafer, before a layer of photo-sensitive material is added. A photomask is then held over the wafer while the entire setup is exposed to a light source, with the photomask blocking light in certain places in order to illuminate the wafer with the intended chip pattern. The wafer is then chemically treated to remove the photo-sensitive layer. Depending on the photosensitive material that is used, either the exposed parts are removed by the solution (positive photoresist), or the unexposed parts are (negative photoresist). The upper oxide layer is then removed in another chemical process called etching.

The final step is to remove the remaining photosensitive material. The chip still needs to undergo many steps in order to become a fully functional product, but a very important one is now complete.

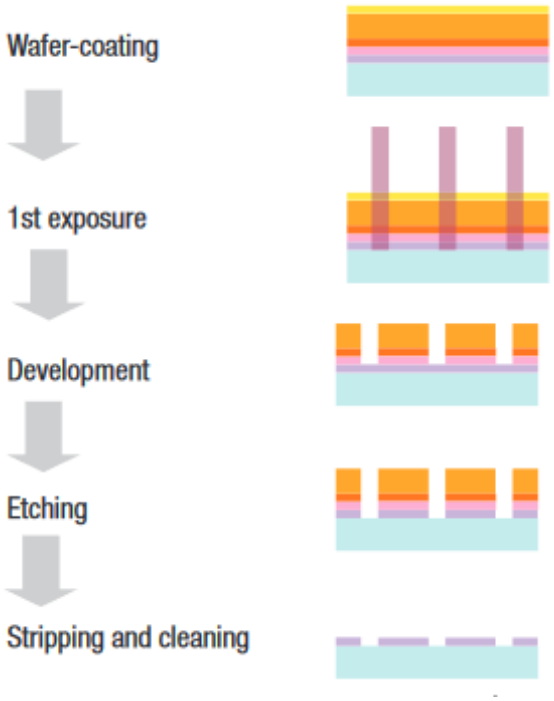

Figure 2: A step by step guide on the photo-lithography process. Image adapted from [4]

As one might expect, the minimum feature length is determined by the wavelength (λ) of the light that is used (as described by the Rayleigh criterion), as well as the lenses used in the setup and a number of other factors [4]. This can be written as follows.

$$\Delta x = \kappa_1 \frac{\lambda}{NA} \tag{1}$$

Where NA denotes the numerical aperture of the lens, and κ_1 a process factor that is determined by the optical system.
Over the years, the development of light sources capable of emitting smaller and smaller wavelengths has been one of the main reasons Moores' law still holds. To illustrate this point: in 1986, Mercury vapour lamps were used to produce light with a wavelength of 436nm. In the 1980s, a large step was made when KrF excimer lasers brought the wavelength down to 248nm, bringing it to the Deep Ultra-Violet (DUV) range. This was further improved upon by the introduction of ArF lasers, which produced light with an even smaller wavelength of 193nm. Only very recently (2018), ASML started shipping its most advanced system yet, the Extreme Ultra-Violet (EUV) system. This machine produces light with an astounding wavelength of just 13.5nm, an enormous leap compared to systems just one generation before [5].
Producing chips under such extreme circumstances is not an easy task however. In order to produce this EUV light, which is very close to soft x-ray radiation, one of the largest chip system manufacturers, ASML, uses droplets of molten tin who are vaporized using a laser in order to turn them into a plasma [6]. This plasma contains highly excited tin particles that eventually relax to a lower energy state, releasing the desired EUV photons in the process. These photons are then collected and guided towards the wafer by a series of mirrors. This process can be seen in figure 3.

Unfortunately, the plasma emits not just the desired photons, but also energetic ions that shoot off in all direc-

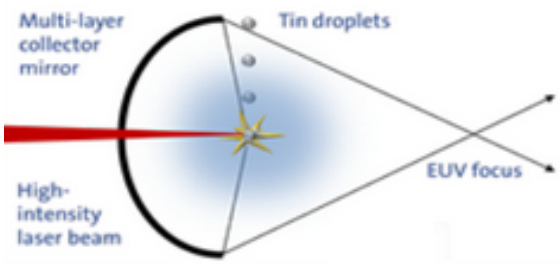

Figure 3: A 2D rendition of the production of EUV photons. Image adapted from [6]

tions. If these ions are not mitigated, they can subsequently interact with any of the mirrors, damaging them and reducing their reflectivity significantly over a short period of time, warranting their replacement [6]. This means the machine needs to be serviced in a special environment, during which there can obviously be no production. The mirrors are also prohibitively expensive due to their complex manufacturing process (each mirror is a dielectric stack [7]) and the extremely high degree of precision with which they are produced.
In order to alleviate this problem, hydrogen gas could be introduced into the plasma chamber as a stopping gas to slow down any ions to the point where they do not reach the mirror, or at least decrease the rate at which defects occur. This relatively simple procedure could extend the lifespan of the mirrors [6].

However, it is not exactly known how tin interacts with hydrogen. For example, how many collisions are there at a given chamber pressure over a certain length? How much energy is exchanged in these collisions?
Questions such as these are what the university of Groningen, in collaboration with ARCNL and ASML is trying to answer.
The university of Groningen is uniquely equipped for this research, as the ZERNIKELEIF facility can generate and select ions (such as tin) with various energies and charges, and let these particles interact with either hydrogen gas, or with a solid sample resembling the mirror used in the actual EUV machines.
The ions are created and energised before they are directed through a beamline towards the experimental setup. Along the way, unwanted ions are filtered out using a magnetic field that is tuned to the desired charge/mass ratio. The beam is also focused at multiple points to prevent it from colliding with the walls of the beamline. Finally, the beam is pulsed before it enters CHEOPS, where the ions interact with hydrogen.
CHEOPS takes Time of Flight (ToF) measurements of the hydrogen fragments that are created in the beam-hydrogen collisions. By simulating the ToF tube in a program called SIMION, we can see how fragments from different source configurations behave within the tube, and use this information to investigate the number of frequency of collisions, and the energy which is exchanged in them.

3 Theory

3.1 Ionic interactions

In the actual setup, a beam of ions (this is usually tin (Sn^{5+}), but other elements and ion charges have also been used) is flown through a chamber in which hydrogen gas (H_2) is released.
The beam ions interact with the target (H_2) to create a number of ionized fragments, transferring electrons from the H_2 to the beam ion. This can be explained according to the over-barrier model. For the example, we'll consider an Sn^{5+} ion and an H_2 molecule.
One can see the two particles in question as two potential wells in which electrons are trapped. If the particles move towards each other, these wells move closer together, and the potential barrier between the wells drops. When the two are close enough, the barrier becomes low enough for one or more electrons to move from the H_2 molecule to the Sn^{5+} ion, where they normally end up in a (transient) lower energy state. This is, in effect, the charge exchange, or electron capture. An example of one such exchange can be seen in figure 4.

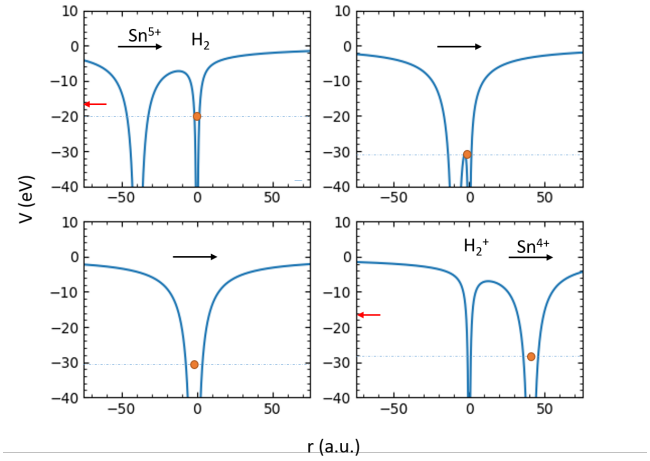

Figure 4: Sn^{5+}–H_2 interaction in terms of potential energy and distance according to the over-barrier model. Note the transfer of the electron

Because Sn is relatively heavy compared to H_2, and in this case has a very high initial energy (around 10keV), the collision will have little effect on its trajectory and velocity. Following a collision, the Sn ion will move on, distancing it from the H_2. This increases the potential barrier between the wells, ending the possibility of further transfer of electrons.

3.2 Collision products

The ionization of H_2 can go a number of ways, depending on how many electrons move between the particles, and how much energy is exchanged. Since H_2 has only two electrons, there can either be a single electron capture, or a double capture.
In the first case, the target can remain either as H_2^+, or as $H^+ + H$, if the amount of energy that is transferred in the capture event exceeds the dissociation energy.

A double capture event will always produce 2 H^+, as the two particles will immediately start to repel one another due to their equal charge. The ions will fly in opposite directions due to the fact that the initial momentum of the H_2 molecule has to be preserved.

According to the Franck-Condon principle, the electron transfers happen within such a short timeframe that the inter-nuclear distances of the involved particles remain the same, in which case we can assume vertical transitions in a potential energy diagram (figure 5) to find the kinetic energy of the fragments.

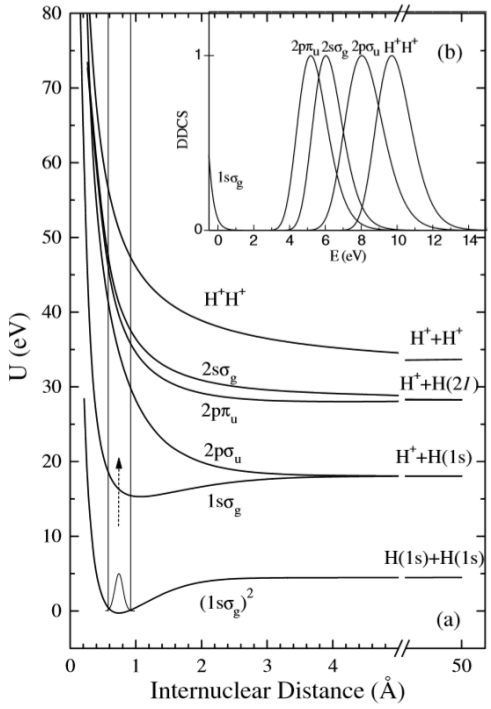

Figure 5: Potential energy curves vs internuclear distance for H_2 and its fragments. Image adapted from [8]

Thus, we can see that there can be a variety of distinct fragments, of which the most important are:
H^+ fragments with a starting energy of 9.7 eV, H^+ fragments with a starting energy of 0 eV, and $H_2{}^+$ fragments with a starting energy 0 eV. The $H_2{}^+$ can possibly be unstable and create H^+ particles with a multitude of energies, but so far these have not been observed in meaningful quantities in experiments with Sn^{5+}. It is assumed this ionization path has a very low probability of occurring with this beam material, and we will not consider it from this point onward due to the scope of this project.
For other beam ion materials, different spectra are recorded, suggesting that these ions produce different target fragments. We will divide the first group of particles in 'forward' ions and 'backward' ions, depending on whether their initial velocity has a component in the direction of the ToF tube, or away from it.

These fragments all have the same charge, but the direction and magnitude of their initial velocity, as well as their mass differ. This leads to them having different arrival times at the measuring device due to the aforementioned velocity, as well as the acceleration of the particle in the electric field. This leads to identifiable peaks when we make a time of flight histogram. The experimental data in figure 6 shows what such a histogram looks like.

We can see that there is an initial area of interest with what appears to be 3 overlapping peaks and a relatively low number of counts. This is the spectrum of the three types of H^+ ions, with the forward ions arriving first, followed by the 0eV ions, after which the backward ions arrive.
Note that the forward peak is higher than the backward peak, even though we know equal amounts of both particles are created.

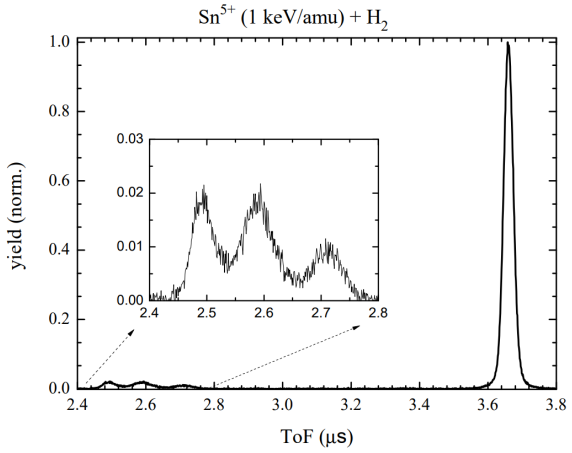

Figure 6: A ToF spectrum showing the full spectrum of H_2 fragments as produced from interactions between Sn^{5+} with energy 1keV/amu and H_2

Then, after around 1000ns with mainly background counts, a much higher peak with a very narrow distribution. These are the $H_2{}^+$ ions, which arrive later because of their mass, being twice as high as the protons.

3.3 Transmission

One of the most important questions we are trying to answer is how frequently the beam ions (that could be Sn^{5+}, or any other ion) collide with H_2 molecules, and in particular, how much energy and charge is exchanged in those collisions.
In order to contribute to answering these questions, the ionized H_2 fragments are extracted by an electric field, accelerated in the time of flight tube, and directed towards a measuring device called an mcp (more on this later, in the section on the experimental setup). In order to enter the tube, the particles have to pass through a diaphragm. The majority of particles don't move through the diaphragm, and are thus not measured. This can clearly be seen in figure 7, where the majority of ions collide with the extraction plate. If the transmission of particles through the diaphragm is known, an estimate of the total number of reactions can be made from the number of measured fragments.

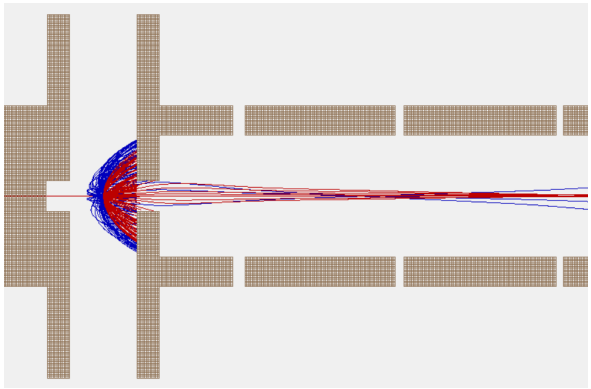

Figure 7: A 2D cut-out of the SIMION model of CHEOPS. Backwards H^+ ions in blue, forward ions in red. Note the amount of ions traversing the diaphragm

As the direction in which an ion flies off when it is created is random, only a small percentage actually makes

it through the diaphragm. From there on, the electric field is tuned so that virtually all of the ions who pass through the diaphragm make it to the detector.

It is possible to mathematically determine this transmission for ions moving through the diaphragm for a point source[9]. Consider a number of H_2 molecules, all of them dissociating into two H^+ ions with the associated initial energy of 9.7eV, moving in a random direction. If we consider all the possible positions of the ions, we can see this as a spherical shell expanding over time, centered around the dissociation site. One half of the shell moves backward, the other moves forward. If we also consider the electric field acting on the ions (this is assumed to be a homogeneous field, generated by a capacitor), the entirety of the shell accelerates towards the negative plate over time. This plate has a hole (the diaphragm) with a radius of 2.5mm, and a depth of 4mm.
One can take T_0 to be the time at which the ions are created. We can then take T_1 to be the time at which all forward ions have either passed the diaphragm, or collided with the extraction plate. We will not consider this latter group as relevant anymore from this point.
We can now calculate T_1, as we know the distance the particle travels in T_1 seconds, which consists of the distance travelled by the centre of mass of the expanding shell due to the electric field (D_1), and the distance travelled because of the initial velocity (D_2).
In figure 8, a 2-dimensional schematic of this can be seen.

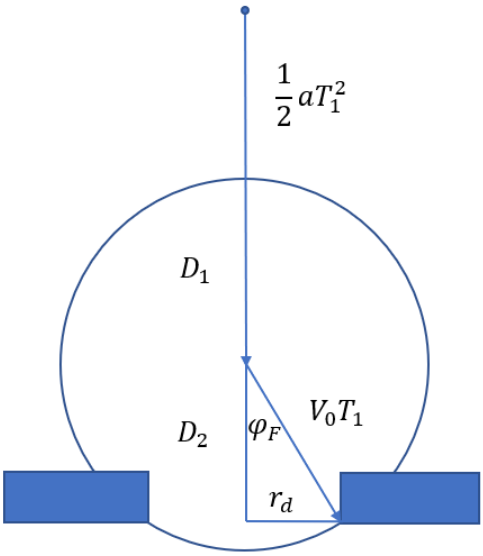

Figure 8: A 2D rendition of the transmission for backwards H^+ ions.

$$D_1 + D_2 = \frac{1}{2}aT_1^2 + \sqrt{(V_0T_1)^2 - r_d^2} = D \tag{2}$$

Here, a is the acceleration the particle experiences because of the electric field.

$$a = \frac{qE}{m} \tag{3}$$

V_0 is the initial velocity of each ion upon creation. It's calculated directly from the well-known equation for kinetic energy (U_i).

$$V_0 = \sqrt{\frac{2U_i}{m}} \tag{4}$$

Here, r_d is the radius of the diaphragm (2.5mm), D the distance between the middle of the ionization chamber and the end of the diaphragm. As the chamber is 10.7mm wide, and the diaphragm is 4mm thick, $D = \frac{10.7}{2} + 4 = 9.35$. Q is the elemental charge of the particle in question, E the electric field over the ionization chamber ($\frac{40}{10.7*10^{-3}}$ V/m) and m the particle's mass.

The trajectory of all of the particles that pass through the diaphragm can be seen to form a spherical cone. This shape consists of a cone with the tip extending from the center of the sphere (dissociation site), combined with a spherical cap. See figure 9 for a visual representation

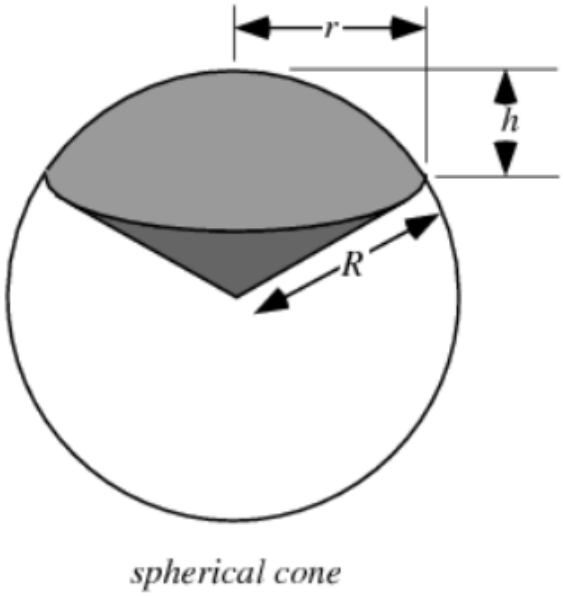

Figure 9: A spherical cone, shown as part of a full sphere

In order to find the area of the spherical cap, we will need the cone angle first.

$$\phi = sin^{-1}(\frac{r_d}{V_0 T_1}) \tag{5}$$

The area of the spherical sector's cap is then readily calculated to be

$$2\pi r^2(1 - cos\phi) \tag{6}$$

All possible directions for forward particles can be circumscribed by a hemisphere. The particles that pass through the diaphragm are then a fraction of that hemisphere, or a spherical cap. The forward transmission (k) can be calculated by dividing the spherical sector's cap area by the area of the hemisphere, which yields the following.

$$k = \frac{2\pi r^2(1 - cos(\phi))}{2\pi r^2} = 1 - cos(\phi) \tag{7}$$

We can use roughly the same equations to calculate the backward transmission, by swapping out T_1 with T_2 (time at which all backward ions have passed the diaphragm), and by changing the sign of the velocity's contribution to the travelled distance to negative.
Figure 10 shows the situation for the transmission of backward ions.

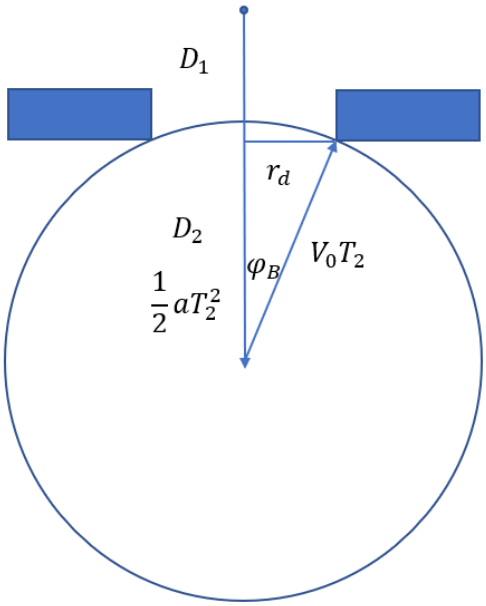

Figure 10: A 2D rendition of the transmission for backwards H^+ ions. Note that the part of the circle beyond the diaphragm does not describe potential ion positions, this is purely to find T_2

$$D_1 - D_2 = \frac{1}{2}aT_2^2 - \sqrt{(V_0T_2)^2 - r_d^2} = D \tag{8}$$

We can then plug in the values and solve both equations to obtain T_1 and T_2, and use those to calculate the transmissions. T_1 is found to be 144ns, T_2 is 377ns. Take note of the difference of the two being 233ns. The transmitted fraction k is then 8.52% , and 1.19% for the forward and backward ions.

The analytical transmission is expected to differ somewhat from the computer simulations which includes the diaphragm due to the fact that the diaphragm will alter the electric field in the simulation, such that it is no longer homogeneous, as is assumed for the calculation.
It is therefore convenient to also see what percentage of ions arrives at the diaphragm, as this can be simulated without altering the field.
This is done simply by changing the total distance D to 5.35mm (substracting the thickness of the diaphragm), and calculating the rates as was done previously. This yields arrival rates of 18.3% and 1.57%.
It is evident that a significant portion of the ions do not make it through the diaphragm, even if they made it to the entrance of the diaphragm.

When considering particles without any initial velocity, the transmission should be 100% for point sources, as the only acting force would be the acceleration due to the electric field, which would push particles directly towards the negative plate in a straight line.
However, if the source is larger than the diaphragm, the transmission is easily found by taking the percentage

of the source that is in front of the diaphragm.

3.4 Delta T

In order to account for accidental measurements and noise, it is possible to filter the data to only count H^+ pairs. If we consider a pair of protons, one directed perfectly in the direction of the mcp, the other in the opposite direction. The direction of the latter ion can be reversed by the electric field, allowing it to reach the mcp as well, albeit somewhat later.

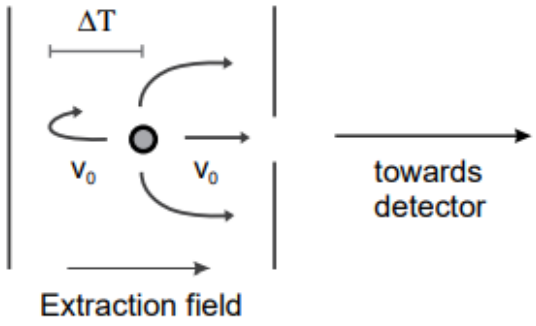

Figure 11: A schematic representation of how the the time difference ΔT between a forward and a backward ion arises. Image adapted from [9]

This time difference, also called Δ T, can be used to filter the data in the following way: after a forward proton has been counted, and an additional proton after Δ T seconds ($\pm$ an error margin), both counts are verified.
Δ T can be calculated using the following formula[9].

$$\Delta T = \frac{\sqrt{8\mu U_{ker}}}{qE} \tag{9}$$

$$\mu = \frac{m_1 m_2}{m_1 + m_2} \tag{10}$$

Where U_{ker} is the total energy released in the dissociation ($2 * 9.7 = 19.4eV$), m_1 and m_2 the masses of the respective particles (in this case, both are protons, so their mass is 1.672*10$^-$27kg), q is the charge and E the electric field through which they travel ($\frac{40}{0.0107}$V/m).
Plugging in these variables gives us a Δ T of 241ns, which is very comparable to the value of 233ns, which was found earlier.

3.5 SIMION

In order to obtain the results we seek, the setup has been simulated in a program called SIMION. SIMION allows users to create a 3D model where they can make a number of electrodes in whatever configuration they like[10].
This goal is achieved by selecting a number of points on a 2D grid to either be electrodes or non-electrodes, and giving the points a set or adjustable voltage. One can also use SIMION to simulate magnetic fields, but this was not of interest to us for this project.
Symmetry axes can be used to simplify the drawing process, in our case by making use of the rotational symmetry of the setup, as it concerns a cylindrical beamline. Only the upper half of a section of the beamline

has to be drawn, which the program will rotate around the symmetry axis to create a 3D cylinder. A simple example is shown in figure 12. This configuration would produce a simple hollow cylinder with an internal diameter of 2 points and an outer diameter of 14 points.

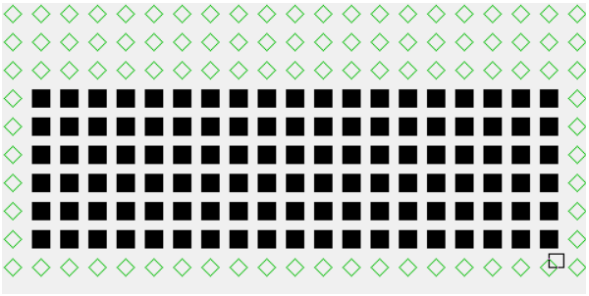

Figure 12: A hollow cylinder as drawn in SIMION using rotational symmetry around the z-axis (aligned along the width of the page)

SIMION then solves the Laplace equation at all points on the grid to approximate the electric field at every point, using the voltages obtained at the nearest 4 points.
You can then create a number of ions that you wish to fly through the setup, combining them into groups. You're able to determine multiple variables for each group, such as the number of particles, their mass, charge, spatial origin, initial energy, initial direction, and a host of other characteristics.
Most of these variables can be defined through either a single value, a distribution, or a set sequence of values. You can have multiple groups in each source type file (.FLY2), and even give each group a colour that allows you to see which group has what trajectory when you record their flight.

One can subsequently let the program record a number of characteristics of the ions at a set instance, for example when the ion starts, comes to a halt at a surface, when it passes a certain plane, or when its velocity changes sign. These characteristics include the ion number (each ion is assigned a number when it is created, this is convenient for identification purposes), the time of flight from creation to measurement, position, velocity, and a number of other variables. For this investigation, the primary variables we are interested in are the time of flight, and the ion number. This allows us to differentiate between multiple groups of ions such as the forward and backward protons, and see what their respective ToF's are.

Once all the ions have gone through their trajectories, the data is compiled in a text file, where each different variable that was measured is recorded in a separate column. Each row represents one ion.
The ToF data can then be loaded into a python script which produces a histogram. The transmission fractions are calculated, by simply counting the measured ions for each group, and dividing them by the initial number of ions.

4 Experimental setup

As mentioned in the introduction, the simulation that is used for this project is based on the experimental setup and the characteristics of the ion beam. This setup consists of several parts, who can be seen in figure 13. Most of these parts are not strictly relevant to understanding how the actual simulation works, but it is still important to know, as one needs to know the assumptions that were made for the model.

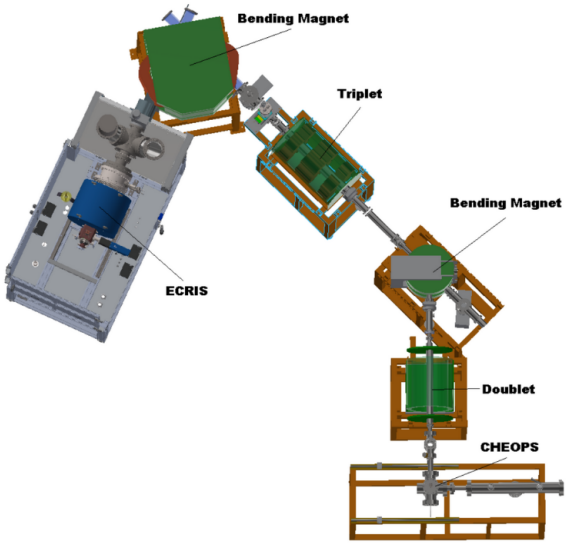

Figure 13: A 3-dimensional rendition of a part of the setup can be seen above. The part of the setup that deals with ion-solid matter interactions is not shown here. Image adapted from [11]

In short, from ion source to experiment: an amount of material (tin, for example) is vaporized and introduced into the ECRIS. Here, the target material is ionised before being pulled out of the chamber towards a magnet which filters out the correct ions through its field. The filtered ions are then focused by a triplet lens before being bent off towards their final destination. Here they are focused again, before being 'chopped' into pulses and let into CHEOPS. In CHEOPS, the ions interact with H_2 to create ionised fragments which are extracted by a field through the ToF tube towards a measuring device called an mcp.
The beam ions are not affected severely by this extraction field and end their journey in a Faraday cup, where their number can be measured.

4.1 ECRIS

ECRIS stands for Electron Cyclotron Resonance Ion Source. As the name suggests, it uses electron cyclotron resonance to energise electrons, who then ionise the beam material. The to be ionized substance is vaporised before being introduced into the plasma chamber. For tin, this is done by heating a crucible filled with the metal, using a filament. Inside of the plasma chamber, electrons rotate due to the presence of a magnetic field which is generated by permanent magnets. Using a radio-frequency source with a frequency of 14GHz, electrons gyrating with the same frequency get energised. Once their kinetic energy is equal to, or greater than the ionization energy of the introduced gas, collisions between the two will start to produce a plasma. Multiple collisions per particle are necessary to create the required charge of the plasma.

4.2 Extracting and focusing

Once the desired plasma state has been reached, the ions need to be removed from the ECRIS. This is rather easily done by means of a puller lens, which is a plate that can be negatively charged to attract the ions and give them the initial velocity required to reach their end goal.
The beam is then focused by means of an Einzel lens. This device consists of 3 cylindrical electrodes. The middle electrode is often set at a positive voltage, while the outer electrodes are grounded. The incoming particle beam will diverge slightly before reaching the middle electrode after which the beam starts to converge. The focal point can be changed by tweaking the potentials, but the first and last electrode must have the same potential.

4.3 110°magnet

As mentioned previously, the ECRIS does not just make one kind of ion, but rather contains a plasma with a host of different ionization states of the target material, free electrons, and possibly some contaminants as well. Think of nitrogen or oxygen from the air. In order to make sure these unintended ions do not make it to the actual setup, the tube through which they move makes a 110 degree bend inside of a tunable dipole magnet. In a magnetic field, electrically charged particles feel the Lorentz force, which is directed orthogonal to the magnetic field line and the direction of the particle at each point. As this force scales with the mass-charge ratio, one can tune the magnetic field to only allow certain ions through. Particles with a different ratio will be either be bent too much or too little, which means they collide with the walls of the vacuum chamber inside of the magnet and do not proceed.

4.4 Triplet

After this, the beam has to be focused again, though this time this is done through the use of magnets.
The name triplet is somewhat misguiding, as it actually concerns a triplet of quadrupole magnets. Each section of the triplet has 4 poles: two north and two south poles, with equal poles situated across each other. The field this produces can be seen in figure 14

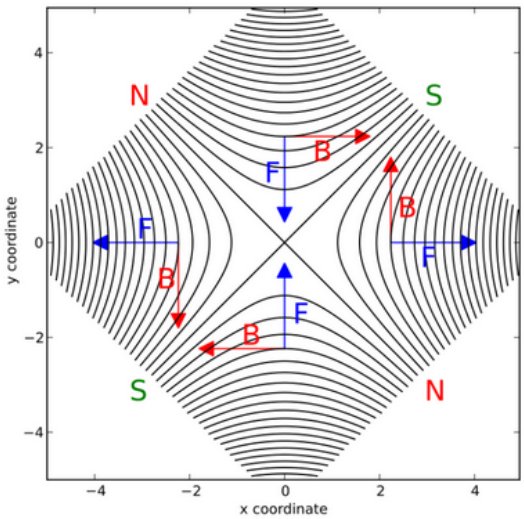

Figure 14: Magnetic field-lines inside of a triplet, with arrows indicating the Lorentz forces acting on the beam. Image adapted from [11]

Due to the Lorentz force, the beam is convergent in one direction, and divergent in another, both of which are orthogonal to the direction of propagation. The beam then enters the next quadrupole, which is rotated 90 degrees with respect to the previous one, thus converging the beam in the plane where it was diverging in the previous quadrupole, and diverging it where it was converging in the previous one. This is then again repeated in the last quadrupole, again rotated by 90 degrees. The fields can be tuned individually to let the maximum amount of ions through.

4.5 45°magnet

This magnet is similar to the 110 degree one that is used for ion beam selection, but it has a different use. The tube splits in two here, with an angle of 45 degrees between them. The straight part goes further downstream the ion beam facility, the branched out beam line goes towards CHEOPS.

4.6 Doublet

This one is similar to the triplet, but instead of three quadrupoles, there are only two. Again, their fields can be tuned for a maximum transmission of ions.

4.7 Chopper Sweeper

Since this experiment concerns the measurement of the time of flight for our ions, there needs to be a starting point at which we can start the time. This task is performed by the chopper. As the name suggests, it 'chops' the continuous beam of ions into short pulses by sweeping the beam over a diaphragm. The pulses pass a 1.5mm diaphragm before they can enter CHEOPS.
There are two plates situated on opposite sides just before the diaphragm. These plates are given an equal but opposite potential (+ and -100), which causes the beam to bent off so much it can no longer move through the diaphragm. The negative plate then becomes positively biased, and vice versa, such that the beam is now deflected the other way (up instead of down, for example). For a brief moment in the transition period, it will have been in line with the diaphragm. When this happens, a pulse of ions passes into CHEOPS, as can be seen in figure 15. The switching happens a couple of thousand times every second.
Every time the potential is switched, a clock starts, and counts are registered for a set amount of time. This produces a 'sweep'. All time sweeps are eventually added together to produce a ToF (Time of Flight) spectrum.

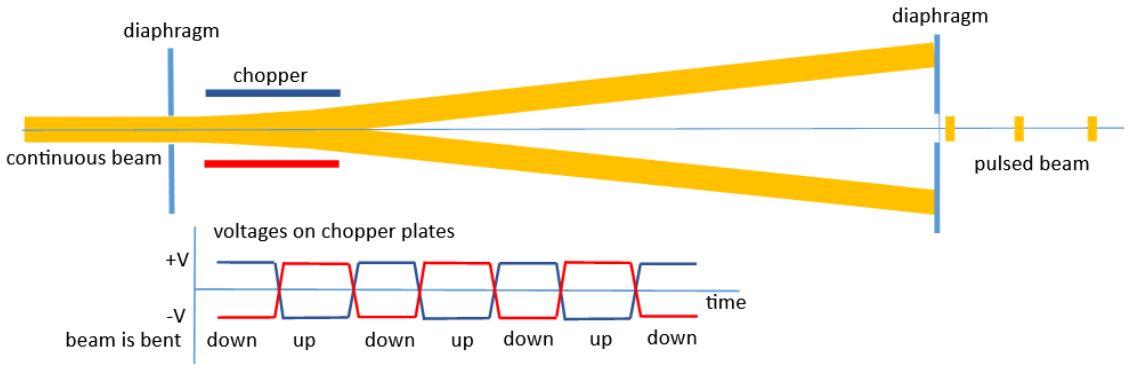

Figure 15: The beam as affected by the chopper sweeper. Also indicated is the voltage of the blue and red plates

4.8 CHEOPS

CHEOPS stands for CHarge Exchange Observed by Particle Spectroscopy.
The ions move through a chamber where hydrogen gas is injected using a thin needle. The beam ions ionize the target (H_2), whose reaction fragments are extracted through a diaphragm and focused using an electric field towards the mcp, where they are registered.

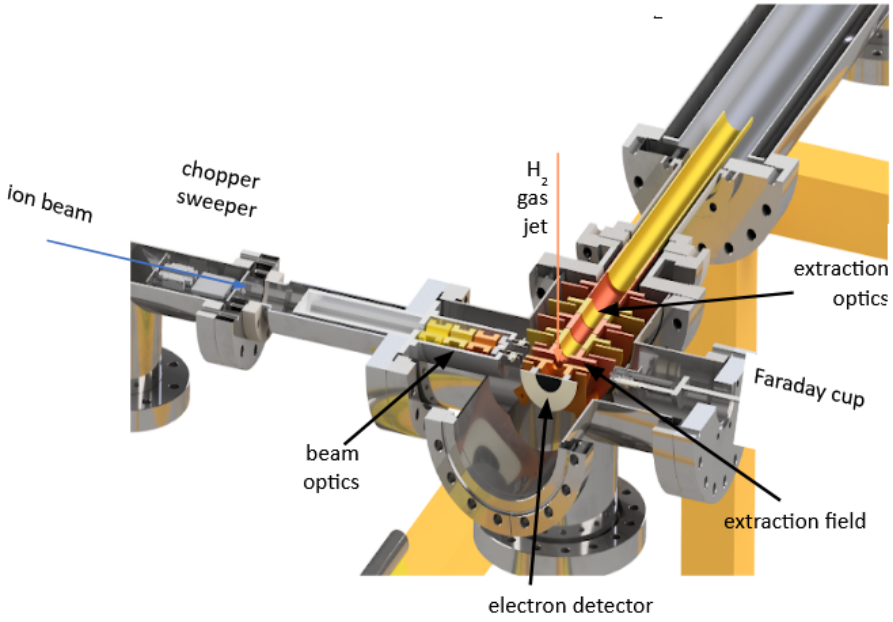

Figure 16: 3D render of the interior of CHEOPS. H_2 gas is injected from above, which is ionised by the ion beam coming from the left. Beam ions are then caught in the Faraday cup on the right. H_2 fragments are transported up towards the mcp, which is not shown here.

4.9 Faraday cup

The beam ions are not affected much by the extraction field due to their mass and velocity. Unlike the hydrogen, they'll continue in an almost straight line towards a collector called a Faraday cup. This device is used to measure the beam intensity.

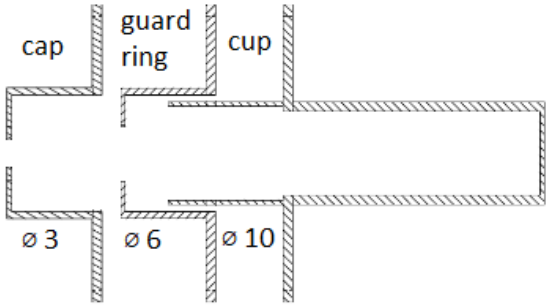

Figure 17: Schematic drawing of the Faraday cup

The device can be simply described as an electrically conductive cup with a guard ring in front of it such that secondary electrons cannot escape the cup. In front of the guard ring is a cap to prevent the voltage of the guard ring from penetrating into the collision chamber. When positive ions hit the cup, they upset the charge balance, causing electrons to be drawn to that region to neutralize it again. This current is measured, and used as a direct measurement of beam intensity. The cup can be moved in both the x- and y-direction to find the position of maximum intensity.

4.10 MCP

The actual measuring device which detects the H_2 fragments is called an mcp, or micro-channel plate. As the name suggests, it is a plate with a large number of microscopic channels. It is quite difficult to detect the minute charge that each ion has, so the channels are made from a material which can emit secondary electrons. Once an ion hits the channel wall, a number of secondary electrons is emitted. These can then hit the wall again and again, releasing an avalanche of electrons. This signal is far more easy to detect than just the single ion that we started out with. As it is more beneficial if the ion hits the wall closer to the opening rather than near the back (this gives more of an avalanche effect), the channels run at an angle, to increase the chance of an early collision.

4.11 SIMION model

4.11.1 Electrode configuration

To properly simulate the ToF tube that is used in the CHEOPS setup, we used a schematic of the tube which had measurements with a precision of 0.1mm. There was an old model that was used by previous students, but it had an accuracy of only 1mm, and was thus lacking in precision.
The current model was made from scratch, the measurements were verified at several instances through the process to make sure they were akin to those from the schematic to prevent mistakes. Voltages were taken from the experimental setup as well. The most important parts of the model, the leftmost and rightmost parts, can be seen in figure 18 and 19, respectively.

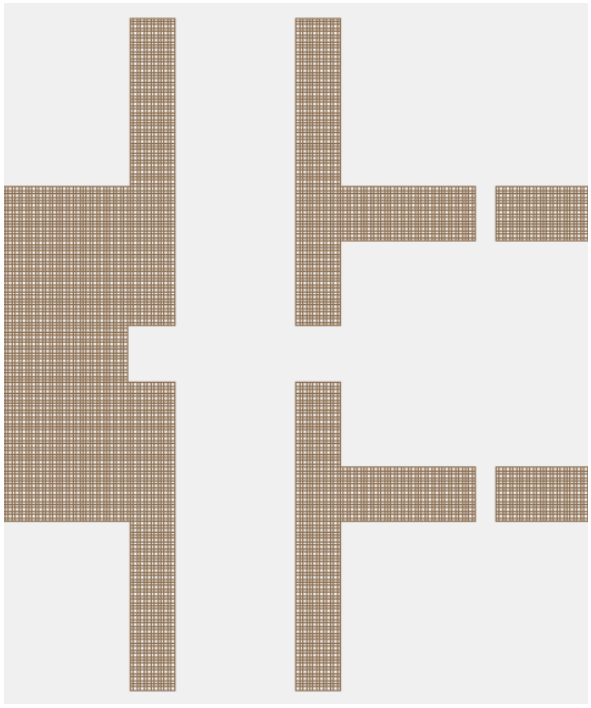

Figure 18: Leftmost part of the SIMION model of CHEOPS. Both the extraction plates, as well as the diaphragm are shown here

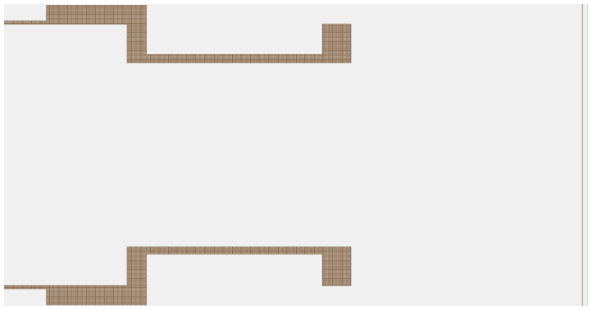

Figure 19: Rightmost part of the SIMION model of CHEOPS. The mcp is visible as a vertical plane on the right

The middle part is not shown here due to the fact that the walls there are so thin that SIMION does not display them, unless sufficiently zoomed in, which would obscure the rest of the model. The geometry of the leftmost part extends into a cylinder with the same diameter as is shown. This cylinder enters a larger one after some distance, which extends into the rightmost portion of the model.

We also modelled a simple capacitor to check if the theoretical model differs from SIMION, as the program assumes certain parameters, while these assumptions may not be made in the theory.
To this end, we constructed a thin plate on the left and a slightly thicker plate on the right that had a hollow section in the middle, 2.5mm high. This hollow section has an inward facing wall-thickness of 1 grid point, with the outward facing wall being thicker, as in figure 20.

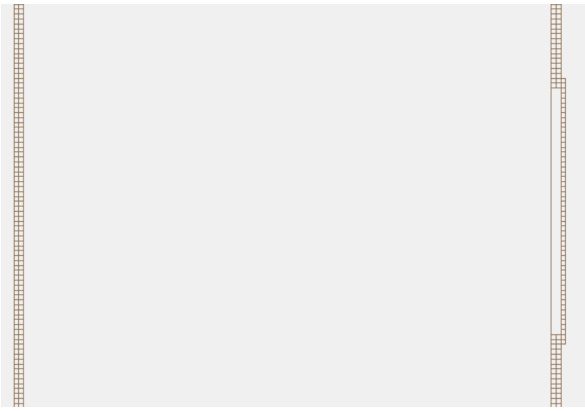

Figure 20: A portion of the capacitor model in SIMION. The thin ”wall” does not stop ions, but does affect the electric field. The detection plane is situated immediately behind this line.

SIMION will not see the 1 point thick wall as an object, allowing ions to move into the plate and beyond a detection plane, just as they would do with the diaphragm. Ions not arriving at this hollow section will see the thicker plate as an object, and will not penetrate it, causing them to not be counted. This thin wall adds to the electric field however, so the aberration caused by the diaphragm is absent.

4.11.2 Source types

We used a variety of sources, each presenting a different configuration of the H_2 fragmentation sites, or source shapes. The first of these is a point source, where ions start out in a single point before propagating in any direction (although the H^+ was subdivided into a forward and a backward group). This source will be the one that is compared to the analytical model, as we assume a single creation site there as well. We also used a point source where the x- or y-coordinate was varied (i.e. the source is moved away from the center), to see the effect this has on the transmissions.
The next source configuration that was considered is a spherical source, with a diameter of 1.5mm, which is the same as the beam diameter in the actual setup, and thus the diameter in which H_2 is ionized. This allows the ions to differ in starting position, creating far less clear-cut results. However, it is closer to what happens in the actual setup.
Finally, we used a cylindrical source, also with a diameter of 1.5mm. This one comes closest to the actual situation, as the chopper sweeper causes the beam to be divided into cylinder-like pulses. These pulses move through the entire length of the chamber, and could thus cause ionization at any point in their wake, which can be seen in figure 21. As most of these fragments would only obfuscate the desired ions in any measurement, we kept the length of our cylinder at 10mm (recall the diaphragm being 5mm wide), sticking out 2.5mm past the diaphragm on both sides.

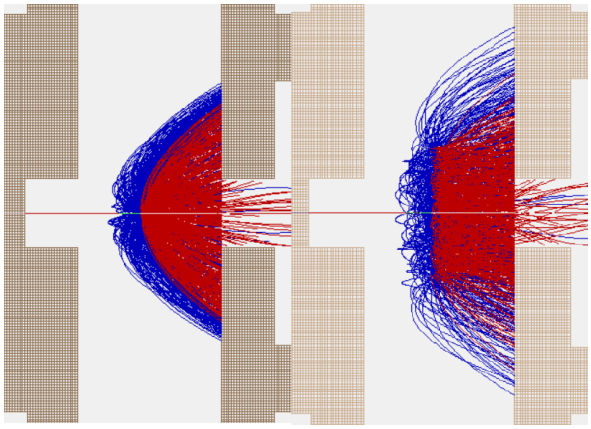

Figure 21: Trajectory of forward (red) and backward (blue) ions as emitted from a cylindrical source, as seen from the side and from the top, respectively.

4.12 Pair sources

The angles dictating the initial direction of the ions is sampled from a uniform distribution. This is not the case in the actual setup, as each ion has a 'twin' which travels in the opposite direction. Due to the large number of ions used (routinely 5- to 10000 per group), the distribution should be dense enough for it to approximate a twin for each ion. However, it is possible to make twin pairs using SIMION, although it takes significantly more effort than simply using a distribution.
Standard source files use groups to describe the ions(.FLY2). These can be converted to files that describe each particle individually (.ION). When this is done, all the values that are taken from a distribution in the .FLY2 file will be input as a single value for each ion in the .ION file [10]. .ION files can be opened as a text file, where each line is an ion, and all its variables are listed one after the other, including the initial angles.
A python script is then used to invert the direction of the ion (Azimuthal angle is decreased by 180 degrees, elevation angle is multiplied by -1), and change the ion colour (this is purely for visual differentiation). The file is then saved as a .ION file again.This then yields a perfect twin for each ion, albeit with a bit of work. This can be done for any type of source, as the starting position will also be set for each particle when converting to a .ION file.
The only drawback to this method is that it takes some time to do, and that the .ION file type only supports up to a 1000 ions. This is not convenient for the type of measurements performed during this project, as such a low ion count would only get a minimal amount of detected hits. One can also not run the same file multiple times, as the .ION files do not recalculate the starting position and direction each time, as happens with the .FLY2 sources. Instead, one has to make however many files in order to get the desired ion count, which is quite a cumbersome process.

5 Results

5.1 ToF spectra

We first made several ToF histograms of H^+ with the different types of sources.
We will be taking a look at the differences and similarities of these histograms, and compare them to the histograms obtained from actual measurements.

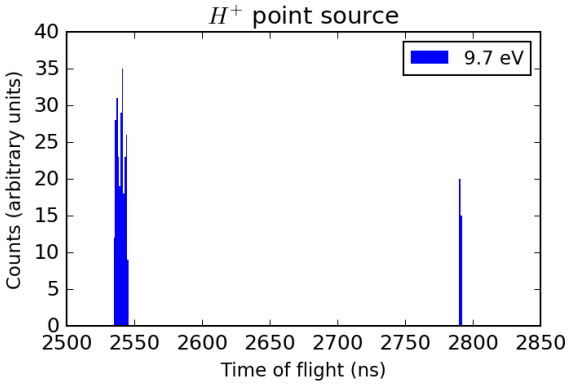

Figure 22: A histogram showing 10000 H^+ ions with an initial energy of 9.7eV as emitted from a point source.

In figure 22, we can clearly see the distinction between the forward and the backward ions in both the time of arrival, as well as the number of counts. Not only do the backward ions arrive later, as expected, they're also fewer in number, also as expected.

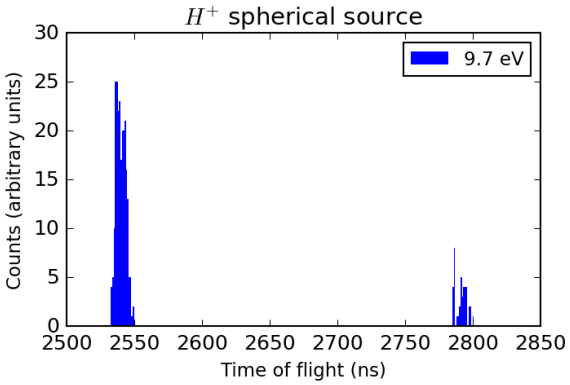

Figure 23: A histogram showing 10000 H^+ ions with an initial energy of 9.7eV as emitted from a spherical source with diameter 1.5mm.

For the spherical source configuration, of which a ToF spectrum can be seen in figure 23, we can clearly see that as the size of the source increases, the distribution of the arrival times also widens. This is due to the fact that there are many more combinations of starting directions and positions, leading to many more possible arrival times.

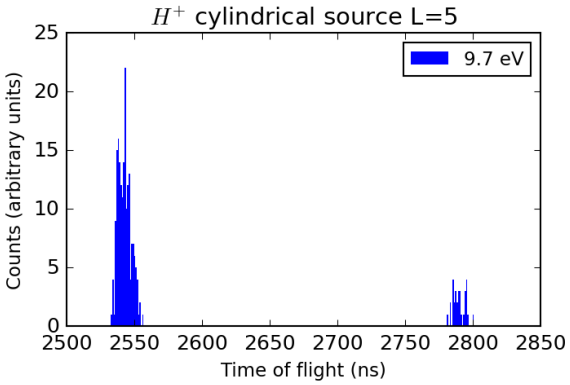

Figure 24: A histogram showing 10000 H^+ ions with an initial energy of 9.7eV as emitted from a cylindrical source with diameter 1.5mm and length 5mm.

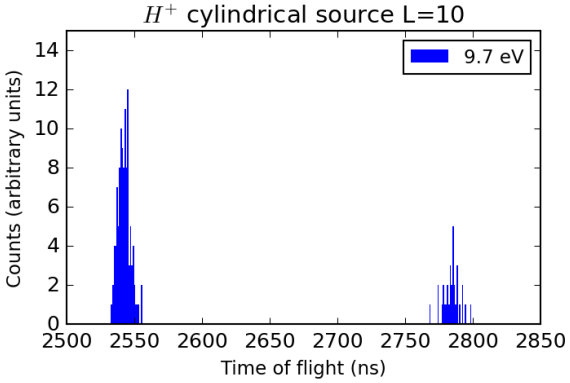

Figure 25: A histogram showing 10000 H^+ ions with an initial energy of 9.7eV as emitted from a cylindrical source with diameter 1.5mm and length 10mm.

What is especially interesting, looking at the backward ions in the cylindrical source of length 5 and length 10 in figure 24 and 25 respectively, is that the peaks seem to broaden. This implies that the backward ions that are created not near the middle, but more towards the ends of the cylinder also have a significant chance of making it to the mcp.

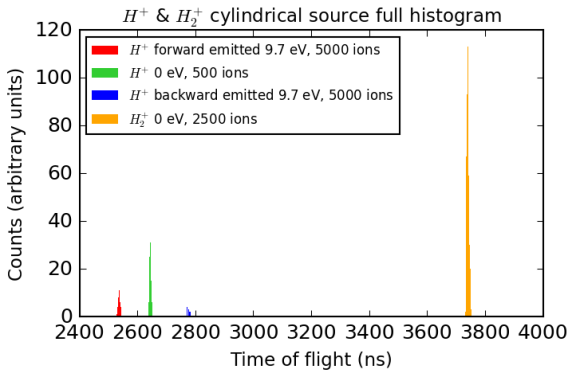

Figure 26: A histogram showing the full spectrum of H_2 fragments as emitted from a cylindrical source with diameter 1.5mm and length 10mm. Note that the number of ions flown differ (see legend)

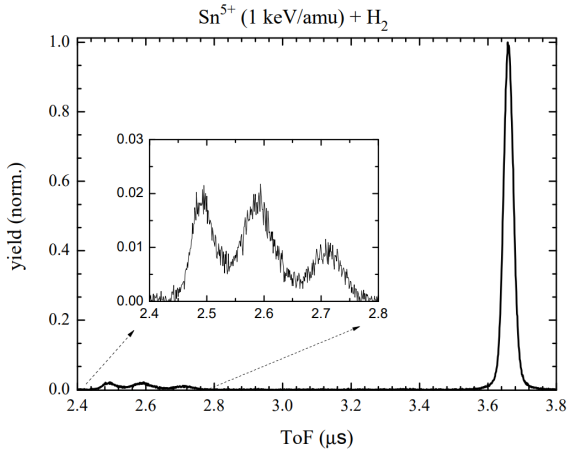

Figure 27: A histogram showing the full spectrum of H_2 fragments as emitted from CHEOPS.

Looking at the full spectrum simulation (figure 26), and comparing it to the experimental data (figure 27), we can already see a couple of things. The H^+ ions arrive in a much tighter spread than they do in the experimental data. Any ratios containing the 0eV H^+ or the $H_2{}^+$ peak surface area should be disregarded, as the initial number of these ions were chosen such that they would match the peak heights found in the experimental data. The 9.7eV H^+ forward/backward ratio, however, is of interest here. For a closer look, we can return to the forward/backward plots, where we can clearly see that the backward ions feature far less prominently than those in the experimental data, where it has perhaps half the surface of the forward peak. This could be because backward ions are still able to pass the diaphragm and reach the mcp even if they are created relatively far from the diaphragm. This would be less likely for forward ions.
Another point of interest is the arrival times of the ions, with the CHEOPS peaks being around 2.5, 2.6, 2.7 and 3.7μs. The simulated full spectrum seems to have something of a delay on it, as all peaks are shifted slightly to the right.
This is perhaps caused by the fact that CHEOPS has to adjust for the time between the chopper starting the clock and the ions actually being produced. If this correction time is overestimated, it could artificially shift the spectrum to the left.

5.2 Delta T

We would like to see if the delta T we found from our calculations is comparable to the ones we find in the simulation. For this, we took two approaches. In the first, we averaged the arrival times of a large number of ions at the mcp for each source, and took the difference between the forward and backward times.
The second method was by using a 'perfect' point source which emitted just two ions: both perpendicular to the electrodes, one heading towards the mcp, the other one perfectly backwards. We again compare the arrival times to find Δ T. This data is recorded in table 1.

	Average forward arrival time (ns)	Average backward arrival time (ns)	Δ T
Point source	2540.4	2791.1	250.7
Spherical	2540.5	2791.6	251.1
Cylindrical (L = 5)	2543.0	2790.0	247.0
Cylindrical (L = 10)	2542.8	2784.3	241.5
Perfect point pair	2536.2	2790.5	254.4

Table 1: Time of arrival for both forward and backward H^+ ions at the mcp, and corresponding Δ T, for a variety of source types. Perfect point pair refers to values obtained for a a forward and a backward ion moving perfectly to and away from the mcp, respectively.

The perfect point source comes surprisingly close to the analytically obtained value of 241ns, considering the fact that the field is not actually homogeneous as was assumed. The averaged values are, expectantly, lower. This is due to the fact that the perfect backwards ion is the most time consuming path, with other paths being faster. We can see that the peaks from the histograms around 2540 and 2790ns for the forward and backward peak, respectively.
We were also interested in the time it took for ions to reach the end of the diaphragm, which can be seen in table 2.

	Average forward arrival time (ns)	Average backward arrival time (ns)	Δ T
Point source	146.3	396.4	250.1
Spherical	146.6	396.8	250.2
Cylindrical (L = 5)	147.7	394.7	247.0
Cylindrical (L = 10)	152.6	387.9	235.3
Perfect point pair	143.2	397.6	254.4

Table 2: Time of arrival for both forward and backward H^+ ions at the diaphragm, and corresponding Δ T, for a variety of source types.

As expected, the time difference for the perfect point pair remains the same. Recount the theoretical T_1 and T_2 of 144 and 377ns respectively. The values obtained from the simulation are again, rather similar.

5.3 Transmission fraction

For the transmissions, we simply divide the number of ions in our output file by the number of ions we flew for each group. This will then represent the fraction of ions that made it past the diaphragm.
In order to see if there is a significant loss of ions between the diaphragm and the mcp, the transmission fraction will be taken at both the diaphragm and the mcp.
Table 3 contains the forward and backward transmission of several source configurations, as well as their ratio. Simulated values have been obtained through flying 30000 ions of each kind, and recording the ones who made it to the mcp.

	Analytic			Simulated			Experimental
	f(%)	b(%)	f/b	f(%)	b(%)	f/b	f/b
Point source	8.52	1.19	7.16	4.65	0.72	6.46	-
Spherical source	-	-	-	4.70	0.77	6.10	-
Cylindrical source (L=5)	-	-	-	4.64	0.69	6.72	-
Cylindrical source (L=10)	-	-	-	4.26	0.76	5.61	2.25

Table 3: Percentage of ions making it through diaphragm, analytical and simulated values for a variety of source configurations. Here, f stands for forward ions, b for backwards ions, and f/b for their ratio

When these ratios are compared to the analytically obtained value, they are somewhat lower. This is due to the fact that the transmission of forward ions is proportionally lower than those of the backward one. As the field is both distorted near the back plate and the diaphragm, these backward ions are affected twice, which could explain the difference.
The ratio is also significantly lower for the cylindrical source with length 10. We can see that the transmission of forward ions is lower, due to the fact they're spread out over a larger length, and thus less likely to pass the diaphragm. The backward ions are not similarly affected, causing a skewed ratio. This is almost certainly the case when looking at the experimental ratio of 2.25. This ratio is grouped with the cylindrical source configuration, which it resembles the most. However, the ratio is roughly a factor 2 lower than its simulated counterpart. We have to note that this ratio is obtained at the mcp, unlike the simulated values, which were obtained immediately behind the diaphragm. The most likely explanation for the difference is the fact that the experimental data also records backward ions who originate relatively far from the diaphragm. This skews the ratio, causing it to be lower. Another explanation could be that the beam is not moving through the middle of the chamber, but is instead propagating at an angle relative to the presumed axis of propagation. This would then have an obvious effect on the transmission, something that is explored in the "source position shift" section of the results.

5.3.1 Arrival fraction

As shown in table 3, there is a slight difference between the analytical transmission and those obtained from the simulation (the latter is 10% lower). This did not come as a complete surprise, as the field in the simulation is far from homogeneous (as the theory assumes) due to the presence of the diaphragm.
We will therefore also compare the arrival rates between the theory and the capacitor simulation, the results of which can be seen below, to see how much the distortion of the field accounts for the difference in transmission.

	Analytic			Simulated		
	f(%)	b(%)	f/b	f(%)	b(%)	f/b
Point source	18.3	1.57	11.66	12.1	0.97	12.5
Spherical source	-	-	-	12.2	1.20	10.2
Cylindrical source (L=5)	-	-	-	11.5	1.02	11.3
Cylindrical source (L=10)	-	-	-	10.1	1.13	8.94

Table 4: Percentage of ions arriving at the diaphragm, analytical and simulated values for a variety of source configurations

The results in table 4 are interesting, as the ratios are now skewed the other way around for the point source. Although both the forward and backward percentages are lower in the simulation, the difference is not proportional. Although the field was in this case ostensibly homogeneous, the numerical approach taken by the program to determine the electric field at each point could have caused an imperfect field, although this difference would have to be small. There is also the very slim chance of SIMION altering the field due to the presence of the ions, though the electric field that would be created by their presence would be dwarfed by that of the capacitor.
We do see that the effect of the diaphragm and the cavity on the left in the CHEOPS simulation has a large effect on the transmission, and that once these factors are removed, that the transmission much more closely resembles the analytical values, so we consider those effects the culprits of the difference.

5.4 Source position shift

One of the reasons why the experimental forward to backward ratio could be off with respect to the analytically obtained value, is if the beam does not actually travel straight through the middle of the ionization chamber. This could alter the transmission of one or more of the ion types.
In order to see if this might be the case, we measured the transmission at various starting position, either shifted in the x or y direction.
We'll start with a source which is shifted in the x-direction, which points through the diaphragm towards the mcp, or to the right in figure 18, 19 and 21. The y-direction is diagonal to this direction, or up in the aforementioned figures.

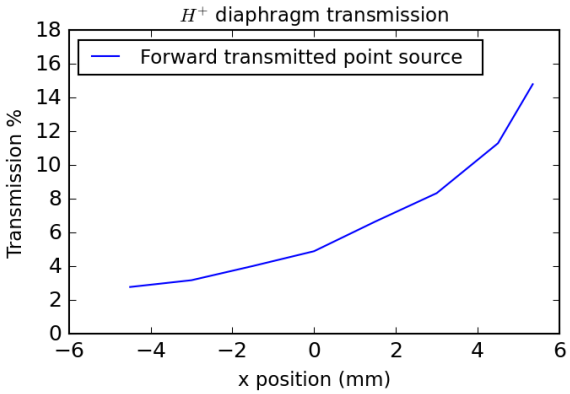

Figure 28: Forward H^+ diaphragm transmission for an x-shifted point source.

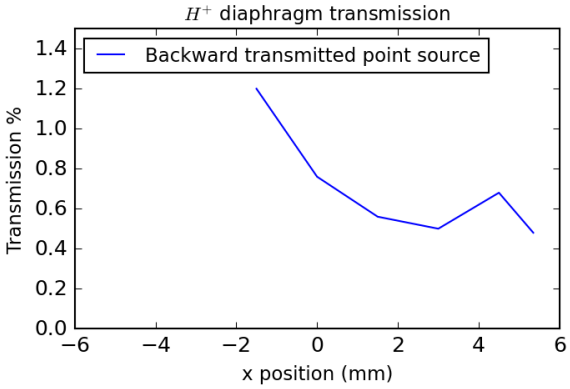

Figure 29: Backward H^+ diaphragm transmission for an x-shifted point source.

Figure 28 reveals that the transmission for the forward ions is behaving as expected; the closer the source is to the diaphragm, the higher the transmission. The relation seems to not be entirely linear, which also falls neatly within expectations.
The backward ions however, exhibit strange behaviour, which can be seen in figure 29. The transmission is initially 0, meaning no ions make it past the diaphragm, before rising to 1.2%. This change is discontinuous, most likely due to the fact that there are no data points in between these two points. Transmission becomes lower as the source moves towards the diaphragm, before going up towards the maximum x-shift and then dropping at the maximum. Needless to say, this is far less straightforward than the trend for the forward ions. The initial lack of ions may be explained by the ions colliding with the back wall before they can turn around, resulting in no ions being detected. The subsequent peaks and valleys are harder to explain, possibly having to do with aberrations in the electric field, caused by the diaphragm and a cavity in the back electrode.

To check this, the simulation has been repeated with a capacitor configuration, which produced the following results.

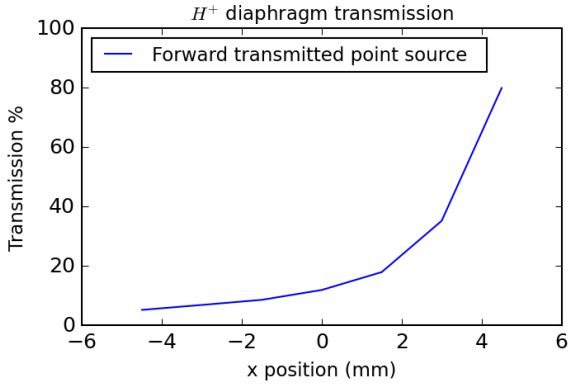

Figure 30: Forward H^+ diaphragm transmission for an x-shifted point source in a capacitor.

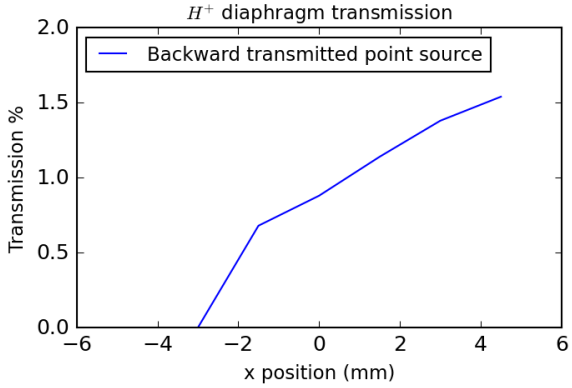

Figure 31: Backward H^+ diaphragm transmission for an x-shifted point source in a capacitor.

The results this produces fall in line with what was initially expected, as transmission increased along with the x-shift. It can still be observed that backward ions who are x-shifted too far to the left collide with the back electrode.

Now, for the y-shift:

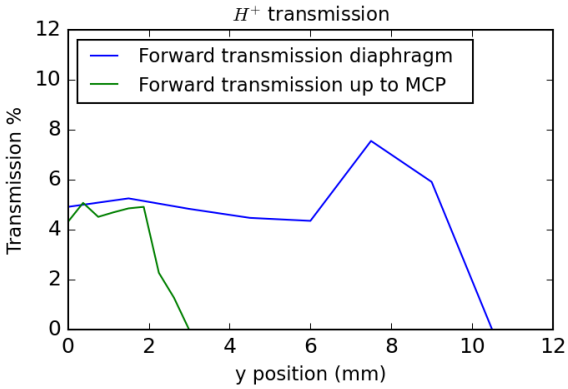

Figure 32: Forward H^+ transmission at the mcp and the diaphragm for a y-shifted point source.

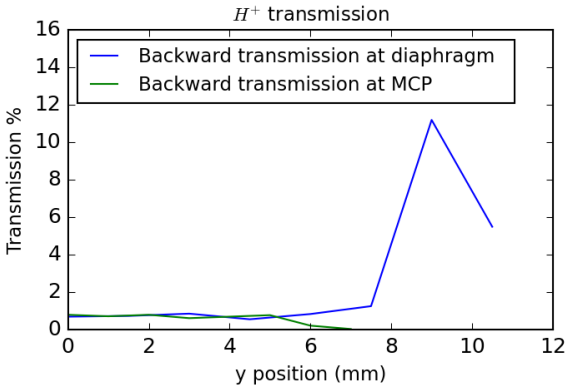

Figure 33: Backward H^+ diaphragm transmission at the mcp and the diaphragm for a y-shifted point source.

As can be seen in figure 32 and 33, the transmission at the diaphragm actually increases as the y-coordinate of the source is shifted a fair amount, before dropping down to zero. This can be visualised as the 'umbrella' of ions that are emitted moves further up along the y-axis, allowing its edge to move over the diaphragm, which increases transmission. Transmission then quickly drops to 0 as the source is now shifted so far none of the ions actually make it to the diaphragm.
This would suggest that either the edges of the umbrella are denser in ions, or the angle larger angle with which they pass the diaphragm allows for a higher transmission.

The measurements were repeated, but this time the transmission was measured at the mcp. figures 32 and 33 shows how this transmission goes to zero a lot faster. The discrepancy is caused by the angle at which the ions enter the diaphragm; even though they have a higher transmission at the diaphragm, they are subsequently more likely to collide with the walls of the ToF chamber. This would explain why they do not reach the mcp.

5.5 Pair production

In theory, once a source has shifted in the y-direction far enough, pairs can no longer be detected as there is no path that would allow both particles to pass the diaphragm and reach the mcp.
We are interested in seeing how the pair detection rate falls off as the source becomes more and more y shifted, in order to see how this compares to the actual setup.

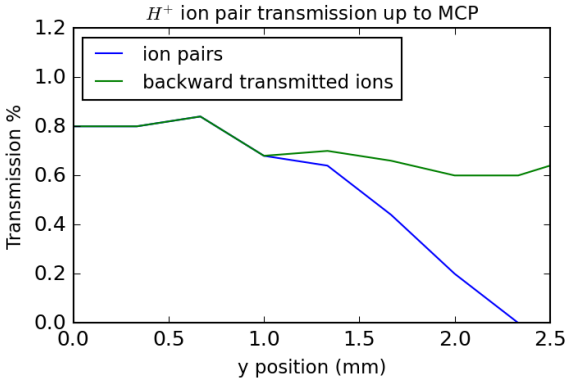

Figure 34: Transmission of backwards ions and pairs vs the y-shift of a point source.

As can be seen, the detection probability falls to zero as the source shifts towards the edge of the diaphragm, while the transmission for backwards ions in general is much less affected by the shift. It is then possible to detect such a y-shift of the source for fairly large shifts. However, due to the relatively small changes and erratic behaviour at small shifts (¡1mm), not much can be said about these smaller changes.

6 Discussion

When we look at the different histograms and compare them to the experimental data, we find that the simulated peaks are much tighter. One of the causes might be due to the fact that the ions were given an initial energy of just one value, instead of a distribution. In the actual experiment the thermal energy of the H_2, as well as the recoil energy from the collision are bound to alter the spread of the arrival times. Both of these energies are rather low however, thermal energy ranging around 25meV, and the collision ¡1eV.
Far more important however, is the bunch length of the beam. As previously mentioned, the beam is chopped into pulses. Collisions cause by Sn^{5+} ions who travel at the back of the pulse arrive later at the mcp than collisions caused by ions who travel at the front. This causes a broadening of the peak by as much time as the length of the bunch (measured in seconds, not meters). This is currently not being modeled, but individual groups can be given a delay, so multiple groups could be used to approximate this. The source which most resembled the one that is being used currently is the cylindrical source, for which a length of 10mm was used most of the time. The beam converges slightly between the chopper and the Faraday cup, its diameter growing from 1mm to 1.5-2mm, which varies between measurements. This is currently approximated by using a diameter of 1.5mm, but it would be interesting to see what kind of spectra a cone-shaped source would produce, if there is any difference at all. However, the difference would most likely be minimal.

As can be seen from the transmission ratios, there is somewhat of a discrepancy between the theory, the simulation and the experimental data (7.16 vs 6.46 and 5.61 vs 2.25 for the point source and the cylindrical source, respectively). The first difference can be explained due to the aberration the diaphragm and cavity cause in the electric field. When the arrival fraction are compared in a homogeneous field, the difference in the ratio almost vanishes completely (11.7 vs 12.5). It is then important to note that the field in the actual setup can't be said to be homogeneous.
The spread in initial energies that was already noted most likely has its effect on the transmission as well, as it would impact the ions' initial velocity. It would be insightful to see how the transmissions change when these factors are taken into account.

When looking at how transmissions changes as the source is moved around, there are a number of points of interest. The position of the beam has (unsurprisingly), a large effect on the transmission. The relation between the position of the source and the transmission is complicated due to the aberrations caused by the diaphragm and the cavity. The y-shift gives relatively small upper bounds to the shift in that direction, as the transmission drops to 0 after just 3 mm. However, this method is most likely not suited to detect smaller changes in the source position, as the transmission remains fairly stable before suddenly dropping off.
It remains to be seen how the transmission changes when both the x- and y-coordinates are changed, as the current investigations have only been regarding the change of one or the other. What is also worth looking into is the simulation of source configurations that are not parallel to an axis. For example, a source that moves down as it propagates, or to the left. This is observed in the experimental data, where the position of the highest beam intensity changes from measurement to measurement.
The Δ T based filtering for pairs offers a more sensitive way to determine possible y-shifts, as the transmission for pairs already drops by 25% at only 1.5mm. It would be interesting to see in what range these values can be found for other source configurations, such as the ones described earlier.

7 Conclusion

Thanks to these SIMION simulations of CHEOPS, several conclusions on Sn-H_2 interactions can now be made. Due to the electric field not being uniform throughout the setup, these conclusions come with a number of caveats, however.
When looking at the spectra, peaks are rather slim compared to the experimental data. This is caused by the fact that not all collisions occur at the same time. Thus, future research could be dedicated to simulating groups of ions with different delays, and comparing the obtained spectra with the experimental data to see how much of the broadening is affected by the bunch length. Optionally, thermal energy and collsion effects could also be accounted for, but as these are much smaller (25meV thermal energy, ¡1eV collision energy), they are not expected to contribute significantly.

The forward/backward ratio of the experimental data is rather low when compared to the simulations (5.61 vs 2.25 for the long cylindrical source). This difference is almost certainly caused by a relatively high number of backward ions, originating far from the diaphragm, being able to pass the diaphragm. These counts can be filtered out by only registering a count if another follows Δ T (250 $\pm$ 10) ns later. More investigation would have to be conducted towards the error, and to see the prevalence of false double counts, as this could be caused by the spread in creation times due to the ion pulse length.
Using the obtained transmissions (4.26% and 0.76% for a 10mm long cylindrical source, for example), it is now possible to make an estimate of the number of interactions that are taking place in the ionization chamber. The previously mentioned thermal- and collision energy also has its effect on the trajectory, and thus the transmission of ions, this is a matter that should also be looked into, to more accurately get the transmission.
It should now also be possible to check the trajectory of the source, using the data for the x- and y-shift of a point source, and pair-filtering to compare the experimental f/b ratio to simulated values. Further research could be dedicated to finding a more general relation between the source position, trajectory and the forward/backward ratio.

8 Acknowledgements

I would like to thank everyone who has helped to write this thesis and perform the research it was based on. This would not have been possible without the help of Ronnie Hoekstra and Subam Rai, my supervisors, and Wouter van Tellingen, with whom I worked together extensively throughout the research project.
I'd like to thank everybody at the lab for making this bachelor project a fun experience, despite the relative lack of face-to-face contact. I would also like to thank Bas Schoonbeek for proof-reading this thesis and providing helpful commentary.

References

[1] 3000-2.html https://www.tomshardware.com/reviews/upgrade-repair pc. Computer history 101: The development of the pc. Accessed: 2021-01-02.

[2] https://www.computerhistory.org/collections/catalog/102650353. Ibm solid logic - progress in electronics: comparison of a vacuum tube, transistor, and a solid logic chip. Accessed: 2021-02-04.

[3] https://www.britannica.com/technology/analysis-of algorithms. Analysis of algorithms, 2011. Accessed: 2021-01-02.

[4] A. Gohnermeier W. Kaiser M. Totzeck, W. Ulrich. Pushing deep ultraviolet lithography to its limits. *Nature Photonics*, 1:629–63, 2007.

[5] https://www.asml.com/en/technology/lithography-principles/light-and lasers. Lithography principles – lights & lasers. Accessed: 2021-01-04.

[6] prof. dr. ir. Ronnie Hoekstra. Exploding microdroplets of tin – the heartbeat of euv-light sources for nanolithography. *Periodiek*, 1:14 – 17, 2018.

[7] M. Ware J. Peatross. *Physics of Light and Optics, 2015 edition*.

[8] S. Martínez et al. H_2 dissociation by h^+ and he^{2+} projectiles at intermediate energies. *Journal of Physics B: Atomic, Molecular and Optical Physics*, 36:4813—4826, 2003.

[9] Hein Otto Folkerts. *Molecular dissociation induced by electron transfer to multicharged ions*. PhD thesis, 1996.

[10] https://simion.com/manual/chap2.html. Chapter 2. simion basics (simion® 8.0 user manual). Accessed: 2021-01-02.

[11] E.E Berends. *Energetic ions traversing hydrogen gas: fragmentation of hydrogen molecules*. PhD thesis, 2019.